EuPA Open Proteomics 8 (2015) 94–103

Contents lists available at ScienceDirect

EuPA Open Proteomics

journal homepage: www.elsevier.com/locate/euprot

Quantitative proteomics and transcriptomics reveals metabolic differences in attracting and non-attracting human-in-mouse glioma stem cell xenografts and stromal cells

Norelle C. Wildburger[a,b,*], Cheryl F. Lichti[b,c], Richard D. LeDuc[d], Mary Schmidt[e], Roger A. Kroes[e], Joseph R. Moskal[e], Carol L. Nilsson[b,c,**]

[a] Neuroscience Graduate Program, Graduate School of Biomedical Sciences, University of Texas Medical Branch, 301 University Boulevard, Galveston, TX 77555-1074, United States
[b] Department of Pharmacology & Toxicology, University of Texas Medical Branch, 301 University Boulevard, Galveston, TX 77555-0617, United States
[c] UTMB Cancer Center, University of Texas Medical Branch, 301 University Boulevard, Galveston, TX 77555-1074, United States
[d] Proteomics Center of Excellence, Northwestern University, 2170 Campus Drive, Evanston, IL 60208, United States
[e] The Falk Center for Molecular Therapeutics, McCormick School of Engineering and Applied Sciences, Northwestern University, 1801 Maple Street, Evanston, IL 60201, United States

ARTICLE INFO

Article history:
Received 25 February 2015
Received in revised form 26 May 2015
Accepted 29 June 2015
Available online 7 July 2015

Keywords:
Glioblastoma
Bone marrow-derived human mesenchymal stem cells (BM-hMSCs)
Mass spectrometry
Cancer proteomics
Transcriptomics
Fatty acid metabolism
Glycolysis
Pentose phosphate pathway
ROS
Glycosylation

ABSTRACT

Bone marrow-derived human mesenchymal stem cells (BM-hMSCs) show promise as cell-based delivery vehicles for anti-glioma therapeutics, due to innate tropism for gliomas. However, in clinically relevant human-in-mouse glioma stem cell xenograft models, BM-hMSCs tropism is variable. We compared the proteomic profile of cancer and stromal cells in GSCXs that attract BM-hMSCs ("attractors") with those to do not ("non-attractors") to identify pathways that may modulate BM-hMSC homing, followed by targeted transcriptomics. The results provide the first link between fatty acid metabolism, glucose metabolism, ROS, and N-glycosylation patterns in attractors. Reciprocal expression of these pathways in the stromal cells suggests microenvironmental cross-talk.

1. Introduction

Glioblastoma (GBM) is the most common adult primary brain tumor [1,2]. Despite an aggressive multimodal therapeutic approach, the median survival rate is approximately one year [2–4]. One of the major factors contributing to the poor outcome of GBM is the lack of therapeutics that can penetrate the blood-tumor barrier to effectively deliver anti-glioma agents [5–8]. To circumvent this obstacle, we and others have utilized bone-marrow human mesenchymal stem cells (BM-hMSCs) for targeted delivery of anti-glioma agents, due to their intrinsic tropism for gliomas following intra-arterial delivery [7–10]. Though the mechanisms underlying BM-hMSC homing to gliomas remain largely unknown, BM-hMSCs are capable of homing to xenografts derived from commercially available "professional" glioma cell lines [7,10], syngenic glioma models [8], and glioma stem cells (GSCs) [11].

GCSs are isolated directly from fresh tumor surgical resections and grown as spheroids in vitro, often expressing CD133 or CD15 cell surface markers [12,13]. These small subpopulations of cells have stem-like properties [12,14]. GSCs are hypothesized to be tumor-initiating cells, responsible for treatment failure due to their stem-like properties, particularly unlimited self-renewal, and their resistance to treatment [12,14]. GSC-derived xenografts (GSCXs),

* Corresponding author at: Norelle C. Wildburger, Dept. of Pharmacology and Toxicology, Dept. of Neuroscience and Cell Biology, University of Texas Medical Branch, 301 University Blvd, Galveston, TX 77555-0617, United States.
** Corresponding author at: Carol L. Nilsson, M.D, Ph.D., Dept. of Pharmacology & Toxicology, CPRIT Scholar in Cancer Research, University of Texas Medical Branch, 301 University Blvd, Galveston, TX 77555-1074, United States. Fax: +1 409 772 9648.
E-mail addresses: ncwildbu@utmb.edu (N.C. Wildburger), clnilsso@utmb.edu (C.L. Nilsson).

http://dx.doi.org/10.1016/j.euprot.2015.06.006

compared to xenografts from commercial rat and human cell lines, offer the highest translational significance as a clinical model of glioma. GSCs faithfully mimic both the genotype and phenotype of the parent tumor in vivo [15]. Though GSCXs are translationally significant [15] and are capable of eliciting BM-hMSC homing, recent work from our group has demonstrated that not all GSCXs elicit BM-hMSCs homing equally [11]. In that study, some GSCXs were able to strongly attract BM-hMSCs after intra-arterial injection, whereas others were unable to attract BM-hMSCs. Those GSCXs that elicited BM-hMSC homing are herein termed 'attractors' while those that do not are termed 'non-attractors'. The attractor and non-attractor phenotypes provide a unique opportunity to understand the mechanisms underlying BM-hMSC homing. That understanding could eventually help identify patients most appropriate for BM-hMSC-mediated delivery.

Previous studies have focused on soluble tumor-derived factors such as PDGF-BB [16], SDF-1 [17], and TGF-β [11] as inflammation-related cues for BM-hMSC homing. These studies have yielded some insight into the mediators of BM-hMSC homing. However, to the best of our knowledge, a mass spectrometry-based proteomic approach has not been applied to decipher the molecular correlates of BM-hMSC homing to GSCXs. Proteins have functions integral to cell–cell signaling, cell structure, and metabolic pathways. Alterations in the proteomic profiles of cells result in the phenotypic characteristics of cancers, such as uncontrolled growth and proliferation, invasion, and metabolic changes to support these features [18,19]. In addition, proteomic alterations in the tumor microenvironment may support malignancies via cross-talk between cancer and stromal cells [20–22]. In principle, high-resolution nLC-MS/MS should allow the distinction between human and mouse proteins on a large scale; identified human proteins would be derived from malignant tumor cells, while identified mouse proteins would represent the stromal component. Therefore, we hypothesized that alteration of the proteomic profile of cancer and stromal cell populations between attractor and non-attractor GSC xenografts may provide insights into key biochemical pathways involved in the attraction of BM-hMSCs to gliomas. We have previously performed label-free quantitative proteomic and targeted transcriptomic studies on GSCs and GBM cells [23–26]. For the first time, we extend these methodologies to attractor and non-attractor GSCXs.

2. Materials and methods

2.1. Chemicals and reagents

LC–MS grade acetonitrile and water were purchased from J.T. Baker (Philipsburg, NJ). Formic acid and radioimmunoprecipitation assay (RIPA) buffer were purchased from Pierce (Rockford, IL). Iodoacetamide (IAA), dithiothreitol (DTT), and ammonium bicarbonate were obtained from Sigma–Aldrich (St. Louis, MO). Sequencing grade trypsin was purchased from Promega (Madison, WI); sodium fluoride (NaF) was supplied by BDH (West Chester, PA), and phenylmethanesulfonylfluoride (PMSF) from Calbiochem (Darmstadt, Germany).

2.2. Animals

Male athymic nude mice (nu/nu) were purchased from the Department of Experimental Radiation Oncology, The University of Texas M.D. Anderson Cancer Center (Houston, TX). Animal manipulations were done in accordance with institutional (MDACC) guidelines under the Animal Care and Use Committee protocols. All approved animal protocols were in compliance with the USDA Animal Welfare Act and the Guide for the Care and Use of Laboratory Animals (NIH).

2.3. Glioma xenograft model

GSCs (GSC11, GSC17, GSC274, GSC268, GSC229, and GSC231) were established as previously described [12,14]. Cells (1×10^6) were implanted into mice via the screw-guide method as previously described [27] for a total of nine attractors (GSCX17, GSCX268, and GSCX274) and nine non-attractors (GSCX11, GSCX229, and GSCX231) as determined from our previous study [11] (Fig. 1).

2.4. Tissue dissection and sectioning

Animals were anesthetized by intraperitoneal injection of ketamine/xylazine solution and sacrificed by CO_2 inhalation. Brains were removed immediately and flash frozen in liquid nitrogen vapor and stored in −80 °C [28]. Brains were sliced 1.5 mm thick encompassing the bolt and injection site using a brain matrix. Tissue punches (1.5 mm diameter; Braintree Scientific, Braintree, MA) for proteomics and transcriptomics were taken from the tumor site within each slice and flash frozen in liquid nitrogen.

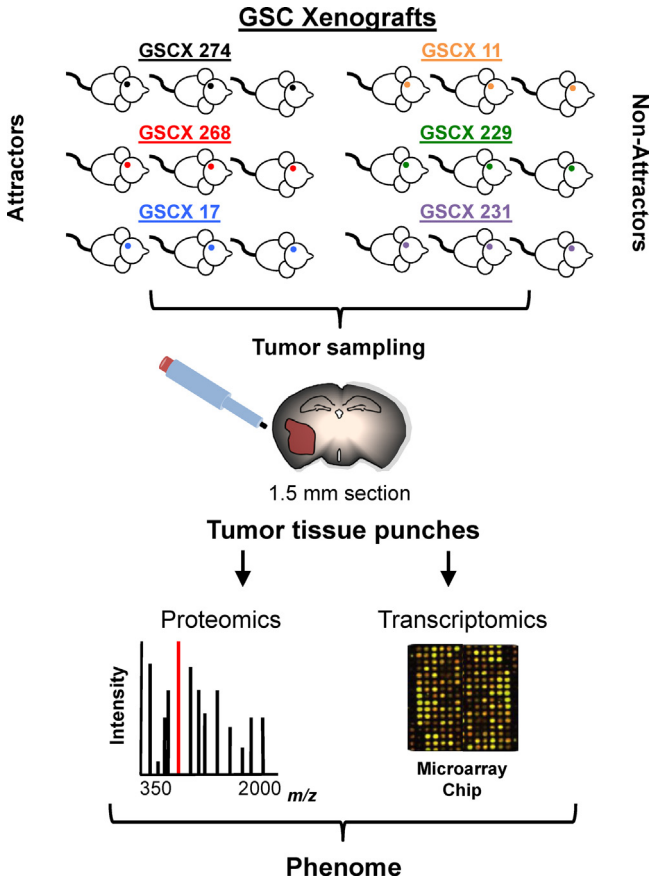

Fig. 1. Workflow for proteomic and transcriptomic analysis of GSC xenografts. Glioma stem cells (GSCs) derived from patient tumors were intracranially implanted into athymic mice. Three of these cell lines represent BM-hMSC homing GSC xenografts (GSCX) (i.e., attractors; GSCX274, GSCX268, and GSCX17) and three represent non-homing GSCXs (i.e., non-attractors; GSCX11, GSCX229, and GSCX231). Nine biological replicates per phenotype were analyzed for statistical inference of biological significance. Brains were removed from tumor-bearing mice and processed for tumor tissue sampling as described in Section 2. Individual tumor tissue punches were processed in parallel for label-free quantitative proteomics and targeted transcriptomic microarray. Quantitative proteomic and transcriptomic data were used to decipher underlying biological differences between the two phenotypes (phenome).

2.5. Protein preparation from brain

Tissue punches were suspended in RIPA buffer containing 2 mM NaF, 2× Halt Protease and Phosphatase Inhibitor Cocktail (Thermo-Pierce), 25 Units of universal nuclease, and 1 mM PMSF (final concentrations). Samples were subjected to seven freeze-thaw cycles each consisting of 90 s in liquid nitrogen and 5 min on ice. Samples were spun for 10 min at 1000 × *g* at 4 °C. The supernatant (whole cell lysate; WCL) was removed and protein concentration measured by BCA (Pierce, Rockford, IL). Whole cell lysates (100 ug) were precipitated with the 2D Clean-Up Kit (GE Healthcare, Piscataway, NJ). Samples were resuspended in 25 mM ammonium bicarbonate (pH 8) with sonication for 5 min. Samples were reduced with 10 mM DTT for 1 h at room temperature and alkylated with 5 mM IAA for 1 h at room temperature in the dark. Proteins were digested overnight with trypsin 1:50 (w/w) at 37 °C.

2.6. Nano liquid chromatography–mass spectrometry

Each individual sample (nine per phenotype) consisting of three biological replicates per cell line were dissolved in 0.1% FA/5% ACN (v/v) and run in a block-randomized fashion (www.random.org) [29]. Chromatographic separations were performed with a nano-LC chromatography system (Easy-nLC 1000, Thermo Scientific) coupled online to a hybrid mass spectrometer consisting of a linear quadrupole ion trap and an Orbitrap (LTQ-Orbitrap Elite, Thermo Fisher Scientific). Samples were loaded on a C_{18} trap column 100 μm ID × 2 cm (New Objective) for online desalting and eluted from a PicoFrit® (75 μm ID × 15 μm tip) column packed with 10 cm ProteoPep II (5 μm, 300 Å, C_{18}, New Objective) with the following gradient at 250 nL/min: 5% solvent B for 5 min; 35% B over 139 min; 95% B over 26 min followed by isocratic at 95% B for 10 min. Mobile phases were 0.1% formic acid in water (A) and 0.1% formic acid in acetonitrile (B). The instrument was operated in positive ion mode for data-dependent analyses (DDA), automatically switching between survey scans (MS) at *m*/*z* 350-2000 acquired in the Orbitrap (60,000 at *m*/*z* 400) in profile mode and MS/MS scans in the Orbitrap in centroid mode (15,000 at *m*/*z* 400). For each sample, the five most abundant precursor ions above a 10,000 count threshold were selected from each survey scan (MS) for HCD fragmentation (isolation width ±2.0 Da, default charge state of 4, normalized collision energy 30%, activation Q 0.250, and activation time 0.1 s as previously described [23,30]). Ion injection times for the MS and MS/MS scans were 500 ms each. The automatic gain control targets for the Orbitrap were 1×10^6 for the MS scans and 2×10^5 for MS/MS scans. Dynamic exclusion (±10 ppm relative to precursor ion *m*/*z*) was enabled with a repeat count of 1, maximal exclusion list size of 500, and an exclusion duration of 60 s. Monoisotopic precursor selection (MIPS) was enabled, and unassigned and singly charged ions were rejected. The following ion source parameters were used: capillary temperature 275 °C, source voltage 2.2 kV, and S-lens RF level 40%. Spectra were acquired using Xcalibur, version 2.0.7 (Thermo Fisher).

2.7. Protein identification

Data files (.raw) were imported into Progenesis LC-MS (version 4.1; Nonlinear Dynamics, Newcastle upon Tyne, U.K) for spectral alignment based on *m*/*z* and retention time using a proprietary algorithm and manual landmarks using one sample ('Mix Control' an equal protein mixture from each sample) as the reference, as previously described [31]. The top 5 spectra for each feature were exported as a combined .mgf file, searched with PEAKS (version 6, Bioinformatics Solutions Inc., Waterloo, ON) against a merged UniProtKB/SwissProt Human Mouse database of canonical sequences (March 2014; 24,541 entries) appended with the Common Repository of Adventitious Proteins (cRAP) contaminant database (February 2012 version, The Global Proteome Machine, www.thegpm.org/cRAP/index.html). The Human and Mouse cRAP database enabled us to identify peptides belonging to either human or mouse as well as peptides with shared sequences in a single database search. PEAKS automatically generated a decoy-fusion, which appended a decoy sequence to each protein for calculation of FDR [32]. All modifications in the Unimod database were considered in the PEAKS search [23,33]. PEAKS searches were performed with a precursor ion mass tolerance of 10 ppm and fragment mass tolerance was 0.1 Da. Trypsin was specified as the proteolytic enzyme and a maximum of two missed cleavages were allowed.

Search results with score (-10log P) of 30 or higher, with an estimated FDR value of <1% (at the protein level) as calculated by PEAKS, were exported from PEAKS and re-imported into Progenesis for manual monoisotopic peak correction. Deamidated peptides identified in the PEAKS database search were used to direct manual monoisotopic peak correction, which is done to correct for misassigned monoisotopic *m*/*z* values not corrected in an automated fashion by Progenesis. After monoisotopic peak correction, the top 5 spectra for each feature were exported as a combined .mgf file, searched with PEAKS and imported into Progenesis for manual conflict resolution. Conflict resolution is the process whereby we ensure that a single peptide sequence is assigned to a single feature, by removing lower scoring peptide assignments to generate a final peptide list with raw abundances as previously described [34]. The peptide list was exported as raw abundances to Excel for data analysis. The mass spectrometric data have been deposited in ProteomeXchange (http://proteomecentral.proteomexchange.org) via the PRIDE partner repository [35] with the dataset identifier PXD001778.

2.8. Proteomic data analysis

All peptides listed as having shared or group accessions, or listed with multiple accessions, were removed—a total of 625 peptides. In this process, peptide sequences belonging to single protein identifications were kept for further statistical analysis while those belonging to more than one (i.e., "shared or group accessions, or listed with multiple accessions") were removed. This criterion (Paris guidelines) increases the confidence of protein quantification [36,37]. Next, all post-translational modifications except carbamidomethylation of cysteine and oxidation of methionine were removed. Mouse and human proteins were sorted and separated before data analysis. Proteins identified as exogenous contaminants, such as keratin and trypsin, were eliminated. Finally, all protein identifications required a minimum of two unique peptides. Proteins without at least two peptides were excluded from further analysis. A total of two tables of peptide intensities (human WCL and mouse WCL) were imported into custom scripts for analysis (Supplementary Tables S1 and S2). All calculations were done using SAS PROC MIXED with restricted maximum likelihood estimations (SAS version 9.4, SAS Institute, Cary, NC), and type 3 sums of squares (where appropriate). In all cases, the intensity of each peptide ion species was normalized by standardization across all measure of that peptide species. Standardization is a calculation in which the average intensity for all measures of a given peptide is subtracted from each measure, and the resulting difference is then divided by the standard deviation of all measures of the peptide. Missing values, defined as the lack of a reported intensity for a given peptide in a given LC–MS/MS run (i.e., a peptide observed in one replicate but not in another), were assumed to be missing at random and were excluded from the analysis. A random effects

model was used to partition variation in the peptide intensities between treatment levels (attractors and non-attractors), the three biological replicates, and the three analytical replicates. Supplementary Tables S3 and S4 contain the results for each protein from each analysis human and mouse, respectively. Next, a hierarchical linear model was used to test for differences in mean intensity between the attractors and non-attractors, while allowing each biological replicate to have its own overall mean. The *p*-values from each analysis were corrected for multiple hypothesis testing with an FDR (q) of $\leq$0.05 considered significant [38]. The same model was run on the $\log_2$ converted raw intensities. The differences in estimated mean between attractor and non-attractor in these tests were taken as an estimate of the overall fold change within the treatment. Supplementary Tables S3 and S4 list the test statistics and effect estimates for each protein interrogated within each analysis. The q-value reported throughout the text is the instantaneous q value (q_inst; Supplementary Tables S3 and S4), which is the FDR if the given protein were taken as the least significant protein differentially expressed. For visualization of data, positive fold change values are indicative of an increase in protein expression in attractors relative to non-attractors and negative fold change values are indicative of a decrease in protein expression in attractors relative to non-attractors. Perseus software (version 1.5.16) was used for visualization the data [39] and the Database for Annotation, Visualization and Integrated Discovery (DAVID version 6.7) for interrogation of enriched [40,41] KEGG pathways [42,43] with a false discovery rate (FDR) of <10% using Benjamini–Hochberg p-value correction (q-value) [38]. The relative $\log_2$ protein fold changes were matched to hexadecimal color codes as previously described [44]. A fold change of +3 corresponded to #FF0000, 0 to #FFFF00 and −4 to #00FF00 for human proteins. A fold change of +3 corresponded to #FF0000, 0 to #FFFF00 and −1.9 to #00FF00 for mouse proteins The proteins and their corresponding color codes were then mapped onto metabolic pathways available in KEGG using KEGG Mapper [42,43].

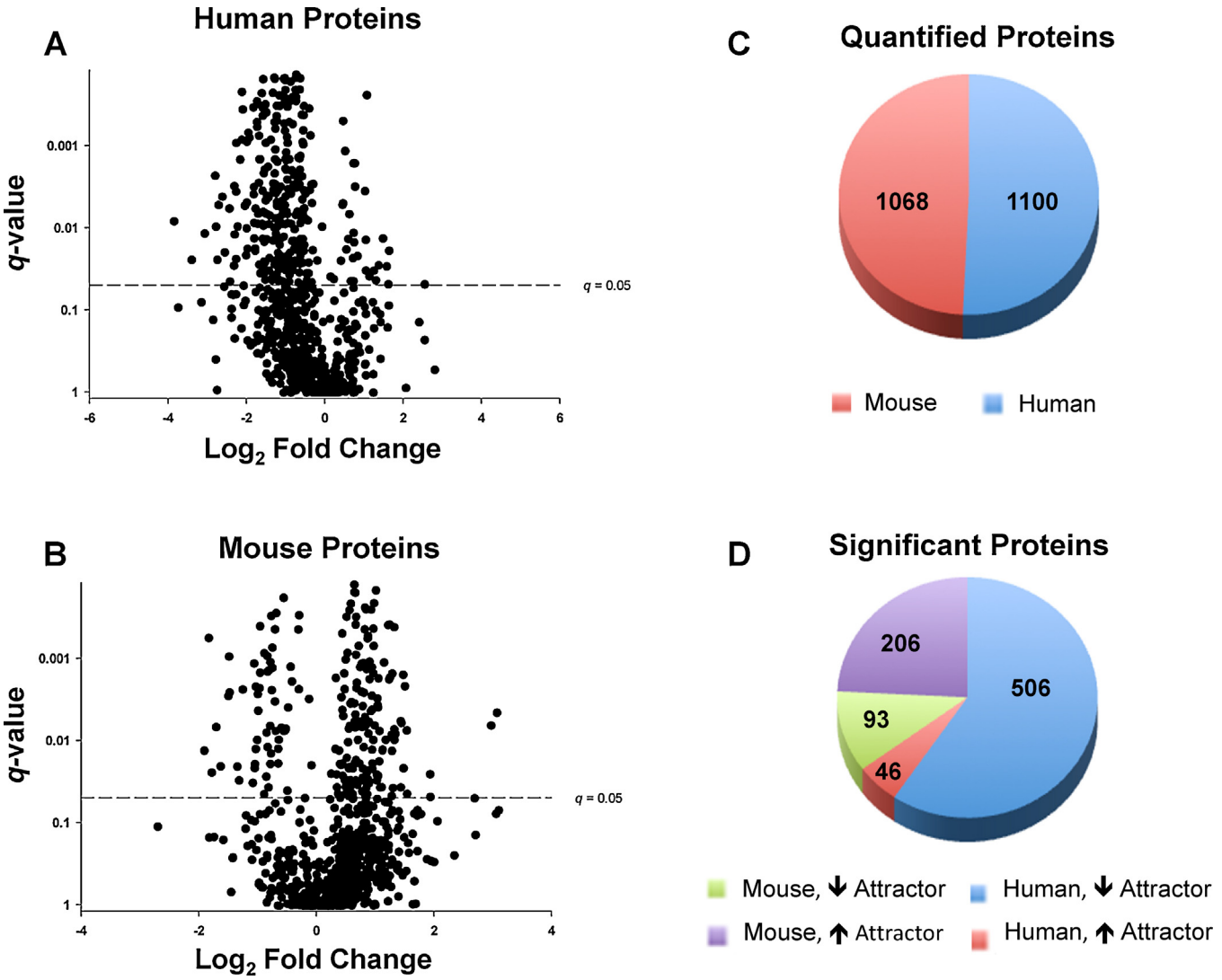

Fig. 2. Volcano plots (q-value vs $\log_2$ fold change) for human tumor and mouse stromal proteins. (A) Logarithmic ratios of attractor (N = 9) vs non-attractor (N = 9) human tumor proteins plotted against the q-value (where $q \leq 0.5$ is considered significant; horizontal line) of the hierarchical linear model. Positive fold change values are indicative of an increase in protein expression and a negative fold change value a decrease in protein expression in attractors relative to non-attractors. (B) Logarithmic ratios of attractor (N = 9) vs non-attractor (N = 9) mouse stroma proteins plotted against the q-value (where $q \leq 0.5$ is considered significant; horizontal line) of the hierarchical linear model. Positive fold change values are indicative of an increase in protein expression and a negative fold change value a decrease in protein expression in attractors relative to non-attractors. (C) Number of quantified human and mouse proteins. (D) Employing a hierarchical linear model (see Section 2) 552 human and 299 mouse proteins were significantly differentially expressed between the attractor and non-attractor phenotype. All proteins are listed in Supplementary Tables S3 and S4 with their respective q-values and $\log_2$ fold change.

2.9. Transcriptomics

A custom targeted microarray containing functional human gene sets related to glioma biology was used to measure the relative expression of epigenetics-, radiation sensitivity-, ion-, metabolomics-, ER stress-, and unfolded protein response-, ubiquitination, chromosome 19-, and all cloned glycogene-related transcripts compiled from the NCBI human sequence and CAZy (www.cazy.org) databases totaling 2577 transcripts [45–47]. Each transcript-specific oligonucleotide was spotted in triplicate on the microarray. A full description of the targeted transcriptomics platform dynamic range, accuracy, reproducibility as well as stringency and quality control measures is available in Kroes et al. [45,46]. The relative quantitation of individual transcript abundance in 18 GSC xenografts ($N = 9$ attractors; $N = 9$ non-attractors) was compared. Briefly, total RNA from each of the defined GSC xenografts was extracted and purified for amplification then labeled with fluorescent dye Cy5 and a universal human reference (Stratagene, La Jolla, CA) was labeled with Cy3 [48]. Microarray chips were scanned using a high-resolution confocal laser (ScanArray 4000XL; Packard Biochip Technologies, Billerica, MA) and Cy3 and Cy5 fluorescence data were analyzed for quality control parameters [45,46] using BlueFuse (Illumina Fulbourn, Cambridge, UK). Significance analysis of microarrays algorithm (SAM, v4.0, Stanford University, Palo Alto, CA) [49] was used with minimum 5000 permutations to determine statistically significant differentially expressed genes. The significance cutoff in these experiments was set to a FDR of $<10\%$ [45–47]. Positive fold change values are indicative of an increase in transcript expression in attractors relative to non-attractors and negative fold change values are indicative of a decrease in transcript expression in attractors relative to non-attractors (Supplementary Table S5).

3. Results and discussion

Mouse tumor xenografts provide a valuable tool as a preclinical model of GBM. GSC-derived xenografts (GSCXs) have a higher translational significance compared to xenografts derived from commonly used commercial glioma cell lines [15]. However, GSCXs exhibiting differential attraction of for BM-hMSCs have not been

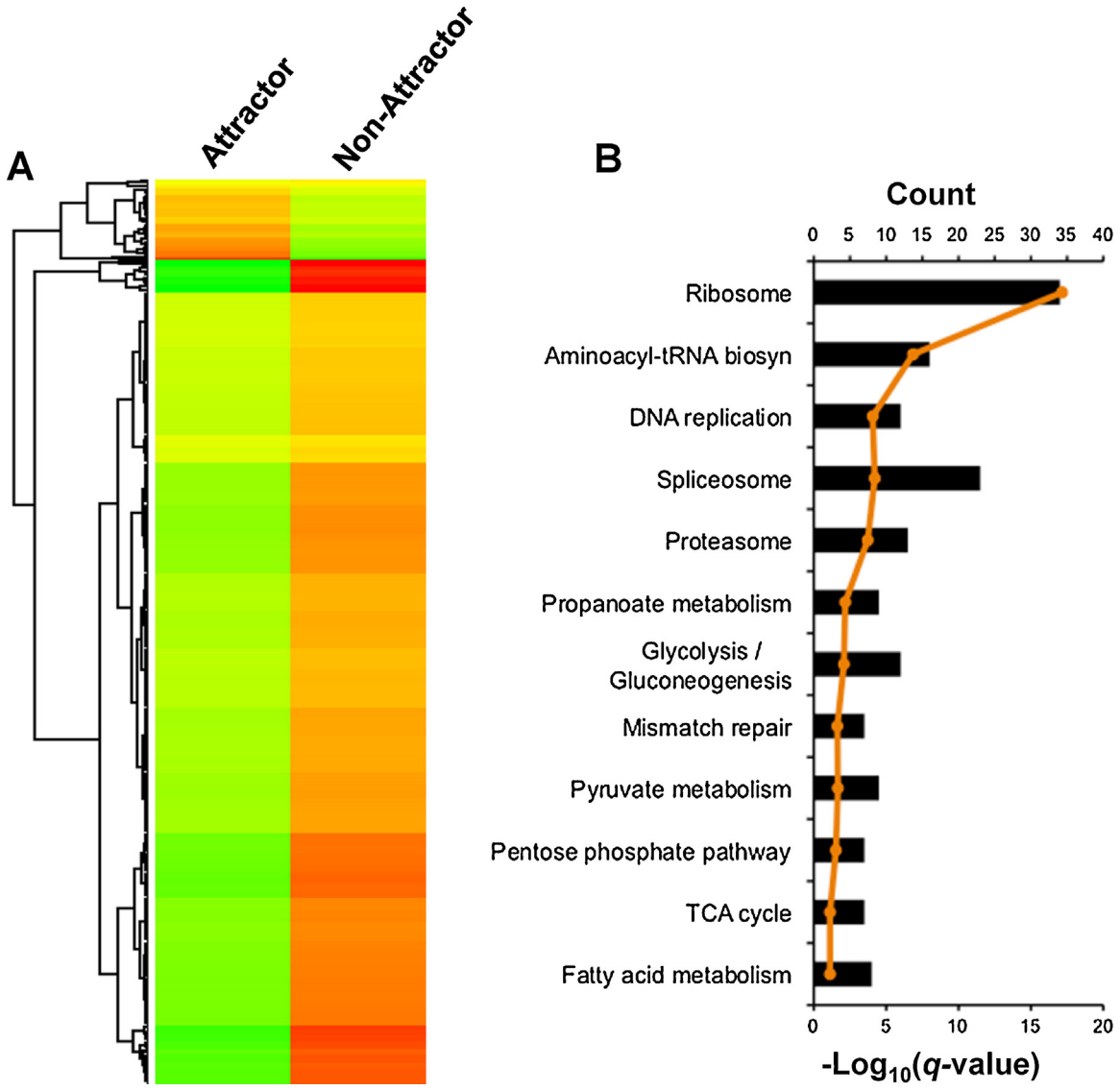

Fig. 3. Analysis of significant human GSC xenograft proteins. (A) Unsupervised hierarchical clustering of all significant human xenograft proteins using $\log_2$ fold change values. (B) Bioinformatic analysis of enriched KEGG pathways using DAVID functional analysis. The top 12 KEGG pathways associated with significantly differentially expressed human proteins are shown. KEGG terms are ranked by the $-\log_{10}$ (q-value) after Benjamini–Hochberg p-value correction (orange line). The black bars show the number of proteins that is common between KEGG term's set and the respective human protein set.

systematically studied at either the proteomic or transcriptomic level. We utilized label-free quantitative proteomics as a reliable technique previously employed by our lab [23,50] that is cost effective, yields high proteome coverage, and does not suffer from dynamic range limitations [37,51]. We also utilized a targeted transcriptomic platform [45–47], which contains genesets related to GBM biology, in parallel to label-free proteomics (Fig. 1). The targeted microarray was used to overcome the limitations of mass spectrometric detection of low abundance proteins (e.g., glycosylation-related enzymes) by measuring gene expression. For statistical rigor of biological significance, nine biological replicates were analyzed per phenotype.

Employing a hierarchical linear model, 552 and 299 human and mouse proteins, respectively were significantly differentially expressed between attractors and non-attractors (Fig. 2). A hierarchical linear model allows us to correctly support the known variance structure within the data with the advantage of being able to detect events of a small magnitude compared to simpler approaches, thus, increasing the number of statistically differentially expressed proteins. Fold changes of small magnitude may have a significant impact on a biological system in reactions with catalytic effect such as metabolism, examined here, particularly if the change occurs at a rate-limiting step. Small magnitude changes in proteins may be critically relevant differences between the two phenotypes.

Within the human tumor protein dataset, 46 proteins were increased in the attractor phenotype and 506 were decreased relative to non-attractors. The mouse protein dataset, which represents the stromal (brain parenchyma) component, 206 proteins are increased in the attractor phenotype and 93 were decreased relative to non-attractors (Fig. 2). We interrogated the KEGG biological pathways using DAVID [40–43] for the 552 differentially expressed human tumor proteins in the heatmap generated by Perseus (Fig. 3A). The top 12 KEGG pathways associated with differential protein expression using a false discovery rate (FDR) of <10% (Benjamini–Hochberg q-value) are displayed with corresponding protein counts (Fig. 3B). Among the top-ranked KEGG pathways were fatty acid metabolism, glycolysis/gluconeogenesis, and the pentose phosphate pathway (PPP). Next we examined the differentially expressed mouse proteins (Fig. 4A) representing the stromal (brain parenchyma) component. DAVID analysis of KEGG

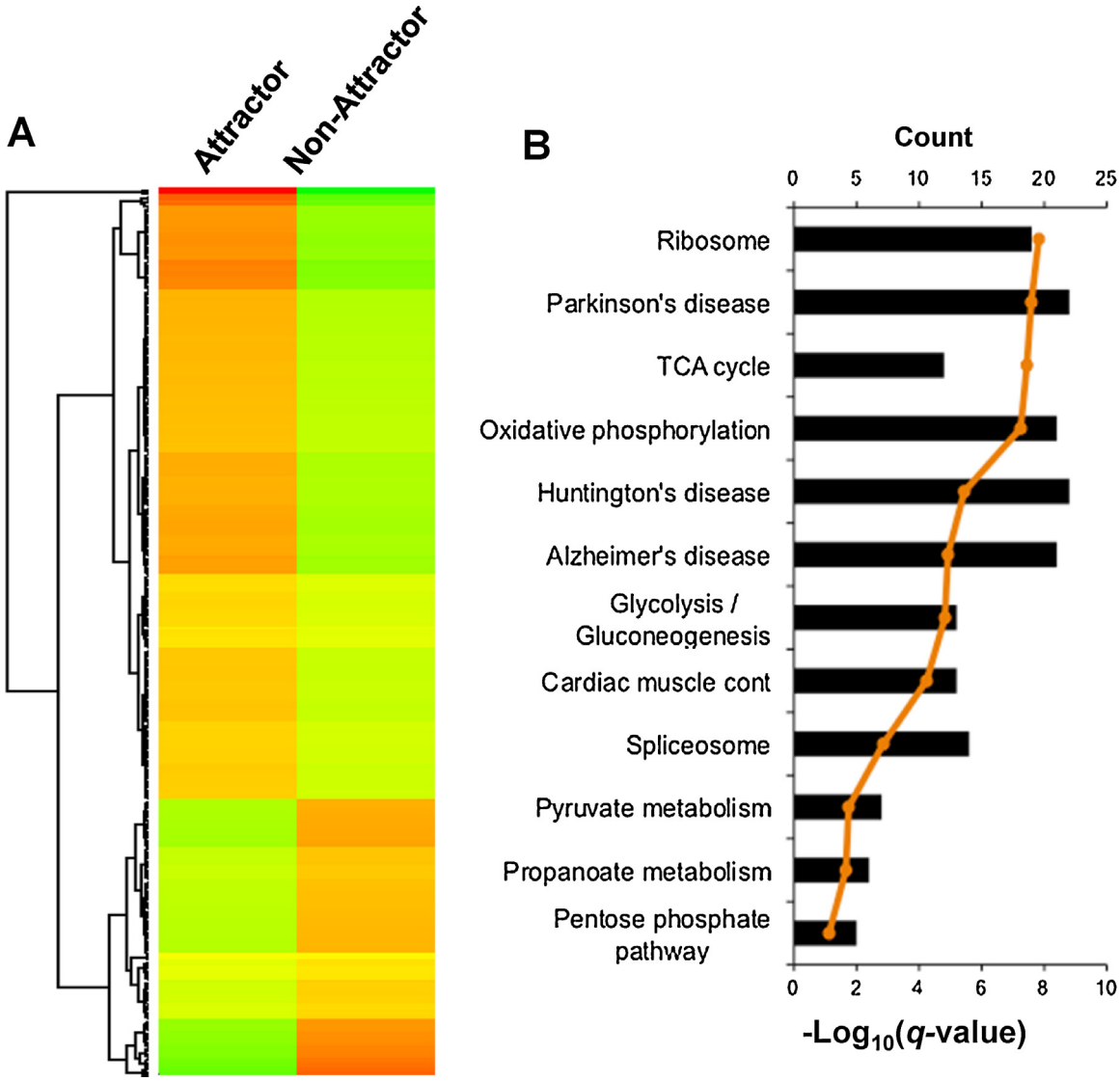

Fig. 4. Analysis of significant xenograft mouse stromal proteins. (A) Unsupervised hierarchical clustering of all significant xenograft mouse stromal compartment proteins using $\log_2$ fold change values. (B) Bioinformatic analysis of enriched KEGG pathways using DAVID functional analysis. The top 12 KEGG pathways associated with significantly differentially expressed mouse proteins are shown. KEGG terms are ranked by the $-\log_{10}$ (q-value) after Benjamini–Hochberg p-value correction (orange line). The black bars show the number of proteins that is common between KEGG term's set and the respective mouse protein set.

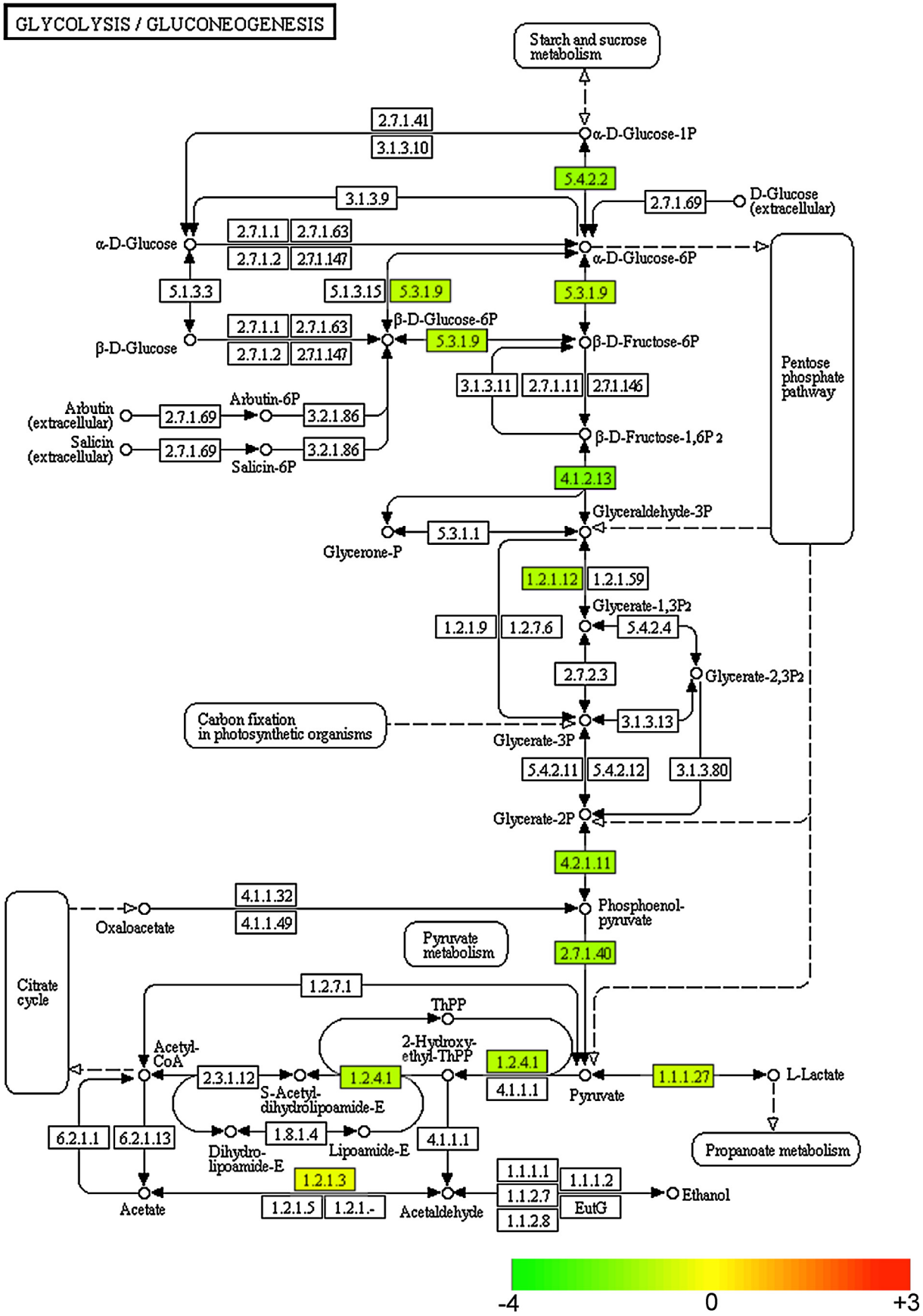

Fig. 5. Human GSC xenograft protein expression values mapped onto the glycolysis/gluconeogenesis KEGG pathway. The human protein expression profiles from GSCXs mapped onto the fatty acid metabolism pathway highlights protein fold changes in attractors relative to non-attractors. The measured protein fold changes were converted to color and mapped onto KEGG pathways. Proteins up-regulated in attractors relative to non-attractors are marked in red, down-regulated proteins in attractors relative to non-attractors are marked in green.

biological pathways [40–43] revealed glycolysis/gluconeogenesis and the PPP among the top-ranked KEGG pathways (Fig. 4B).

3.1. Fatty acid metabolism

In order to determine how fatty acid metabolism differs between attractors and non-attractors, the $\log_2$ protein fold change values were converted to hexadecimal color codes and mapped onto the KEGG pathway [44]. The mapped protein expression data showed an overall decrease in the KEGG fatty acid metabolism pathway in the attractors relative to the non-attractors (Fig. S1). Docosahexaenoic acid (DHA), one of the most abundant fatty acids in the CNS [52,53], is a member of this pathway. As seen in Fig. S1, there is a decrease in relative expression of proteins involved in DHA synthesis in attractors (e.g., trifunctional enzyme subunit alpha and very-long-chain enoyl-CoA reductase), as well as many upstream enzymes indirectly involved in DHA synthesis including: acetyl-CoA acetyltransferase, hydroxyacyl-coenzyme A dehydrogenase, enoyl-CoA hydratase, and fatty acid synthase.

DHA is a precursor to many bioactive molecules with anti-inflammatory effects [54–58]. Our lab has previously shown, using ESI–MS/MS and MALDI-IMS followed by MALDI-MS/MS, that DHA, the precursor to inflammatory-resolving molecules, is decreased in the attractor phenotype [59]. The fact that the proteomic data from our xenografts is congruent with our previous lipidomic analysis on these samples adds a level of confidence to our dataset, providing orthogonal validation to the lower expression levels of the DHA observed in attractors. The decreased levels of DHA and the proteins responsible for its synthesis may be a key component to the homing permissive environment of attractors [59].

3.2. Glycolysis and the pentose phosphate pathway

Glycolysis is a cancer-related pathway [18,19], and its enrichment in our bioinformatic analysis via DAVID is a validating measure in our xenograft tumor samples. A characteristic feature of transformed or malignant cells is a metabolic shift toward glycolysis, first described by Otto Warburg [60,61]. The glycolytic shift in tumor cells is independent of defects in mitochondrial respiration and oxygen availability [18,19]; gliomas are no exception to this phenomenon. GBM cells have been observed to convert 90% of glucose to lactate and alanine via glycolysis in vitro [62]. To understand the regulated changes in glycolysis between attractors and non-attractors, we mapped the $\log_2$ protein fold change values of human tumor proteins to the KEGG glycolysis pathway. We found that in the attractors, the glycolytic pathway was down-regulated relative to non-attractors (Fig. 5). The attractor stromal microenvironment, on the other hand, had reciprocal expression of glycolysis. Glycolysis was up-regulated in attractors relative to non-attractors (Fig. S3A).

The down-regulation of glycolysis in attractors prompted us to consider the status of other glucose-dependent pathways. Glucose, upon entering the cell through glucose transporters and phosphorylated by hexokinases, may also be consumed by glucose-6-phosphate dehydrogenase (G6PDH) and converted to 6-phosphogluconolactone, thus entering the PPP [63]. The PPP is a biochemical pathway that metabolizes glucose to produce NADPH for fatty acid metabolism, redox reactions, and ribose 5-phosphate for nucleotide synthesis. Up-regulation of the PPP has been posited to provide a selective advantage to cancer cells [64,65]. We examined the protein expression profile of GSCXs in the PPP, which notably was also a KEGG pathway enriched in our analysis (Fig. 3B). Mapping the $\log_2$ protein fold change values of human tumor proteins to the KEGG pentose phosphate pathway, we observed that the PPP was also down-regulated in attractors relative to non-attractors (Fig. S2). Notably, G6PDH, which catalyzes the first and rate-limiting step in the PPP, and 6-phosphogluconolactonase, another key enzyme in the oxidative branch, were decreased in attractors (Supplementary Table S3). Transketolase, a component of the non-oxidative branch in the PPP, was also decreased in attractors (Fig. S2) [18,63]. The down-regulation of the PPP would suggest compromised defense against reactive oxygen species (ROS) in attractors compared to non-attractors. Consistent with this, we found a down-regulation of glutathione S-transferase and superoxide dismutase in attractors relative to non-attractors. In addition, the down-regulation of the PPP in attractors would reduce the NADPH production necessary for fatty acid synthesis [66]. Congruent with this, the fatty acid metabolism pathway, as described above, is concomitantly decreased in attractors relative to non-attractors.

Similar to glycolysis, the attractor stromal microenvironment had reciprocal expression of glucose-dependent metabolic pathway, PPP (Fig. S3B). Taken together, our findings suggest microenvironmental cross-talk between the tumor and the stroma. This is supported by several reports of the microenvironment supporting tumor growth, survival, and metastasis [20–22]. The possibility of stromal cell support via reciprocal expression of glucose metabolism may point to a role for the stroma as an important component in BM-hMSC homing.

3.3. Glycosylation targeted transcriptomics

Glucose is the primary carbon source for fatty acid metabolism, glycolysis, and the PPP [18]. With the down-regulation of all three of these pathways in attractors, it is possible, though not mutually exclusive, that either attractors have decreased glucose transport across the cell membrane, or attractors are shunting glucose toward the hexosamine biosynthesis pathway, which is responsible for generating activated sugars for glycosylation [67–69]. To gain insight into the latter possibility, that glucose metabolism may be shifted toward the hexosamine pathway, we used a custom microarray platform containing 2577 transcripts [45,46].

Microarray analysis revealed 254 genes that were significantly differentially expressed at $<$10% FDR. Of the 254 differentially expressed transcripts, 121 had increased expression in attractors relative to non-attractors and 133 had decreased expression in attractors relative to non-attractors (Supplementary Table S5). Glutamine fructose-6-phosphate amidotransferase 1 (*Gfpt1*), which controls the flux of glucose into the hexosamine biosynthesis pathway along with (*Gfpt2*), was down-regulated ($-$1.28-fold) in attractors. Yet, enzymes involved in the N-linked glycosylation pathway synthesis, dolichol-phosphate mannosyltransferase subunit 1 (*DPM1*) and dol-P-Man:Man(7) GlcNAc(2)-PP-Dol alpha-1,6-mannosyltransferase (*ALG12*), had increased expression in attractors relative to non-attractors (Supplementary Table S5) [69]. Dolichyl-diphosphooligosaccharide-protein glycosyltransferase (*STT3B*), which catalyzes the transfer of the high mannose lipid-linked oligosaccharide to nascent polypeptides, was up-regulated 1.33 fold in attractors [69]. Enzymes involved in the biosynthesis of complex-type N-glycans beta-1,4-galactosyltransferase 5 (*B4GALT5*) and the commitment step of complex N-glycans, alpha-mannosidase 2$\times$ (*MAN2A2*) were 1.27 and 1.21 fold up-regulated, respectively. The transcript *NGLY1* encoding the enzyme commonly known as PNGase F, which removes N-linked glycans, was down-regulated ($-$1.35 fold) in attractors relative to non-attractors.

The expression of these significant human glycogenes found in our targeted transcriptomic dataset provides evidence that N-linked glycosylation is increased in attractors relative to non-attractors based on key enzymes responsible for N-glycan processing, the commitment step toward complex-type N-glycans, and the transfer to nascent proteins. Additionally, the enzyme responsible for N-glycan hydrolysis (*NGLY1*) was down-regulated. The relevance of

cell-surface glycosylation in brain tumors [70] warrants further glycomics-based investigation of the tumor cell surface.

4. Conclusions

We showed a decrease in the human proteins responsible for fatty acid metabolism in attractors compared to non-attractors. The predicted outcome of this would be a decrease in the biosynthesis of DHA in attractors, which supports our previous lipidomic study [59]. We also show an overall down-regulation in glucose-dependent metabolic pathways – glycolysis and the PPP – in attractors relative to non-attractors. A consequence of such regulation is decreased NAPDH for fatty acid metabolism and homeostasis of ROS. Despite the decrease in glucose-dependent metabolic pathways, we found an increase in glyco-transcripts involved in glucose-dependent N-linked glycosylation in attractors relative to non-attractors. Finally, our data reveals an up-regulation of glucose-dependent metabolic pathways in the mouse stromal component in attractors relative to non-attractors, in contrast to the human tumor proteins. Taken together, these results implicate lipids and ROS in glioma-induced BM-hMSC homing and suggest a role for tumor microenvironmental cross-talk.

Author contributions

N.C.W. conceived of the study, designed, and performed all proteomics and transcriptomics experiments, data analysis and interpretation, and wrote the paper. C.F.L. contributed to the experimental design, interpretation of data, provided tools for data analysis and contributed to writing the manuscript. R.D.L. performed statistical analysis on proteomic data. M.S. assisted in transcriptomics experiments and data analysis. R.A.K. and J.R.M. contributed transcriptomics data analysis tools and provided helpful discussion. C.L.N. conceived the project and supervised the work and critically revised the manuscript. All authors read and approved the final manuscript.

Conflict of interest

The authors do not have any conflicts of interest to disclose.

Acknowledgements

The authors gratefully acknowledge the financial support of the Cancer Prevention Research Institute of Texas (CPRIT) and The University of Texas Medical Branch to C.L.N. as well as the Dr. Ralph and Marian Falk Medical Research Trust to J.R.M, are gratefully acknowledged. The authors would like to thank Dr. Ekaterina Mostovenko for the R script for visualizing $\log_2$-transformed expression values as hexadecimal color codes. The authors gratefully acknowledge Dr. Frederick F. Lang and Joy Gumin for the glioma stem cell xenografts (GSCXs) at MD Anderson Cancer Center for this study.

Appendix A. Supplementary data

Supplementary data associated with this article can be found, in the online version, at http://dx.doi.org/10.1016/j.euprot.2015.06.006.

References

[1] P. Kleihues, H. Ohgaki, Primary and secondary glioblastomas: from concept to clinical diagnosis, Neuro Oncol. 1 (1) (1999) 44–51.
[2] D.N. Louis, et al., The 2007 WHO classification of tumours of the central nervous system, Acta Neuropathol. 114 (2) (2007) 97–109.
[3] M.E. Berens, A. Giese, . . . "those left behind". Biology and oncology of invasive glioma cells, Neoplasia 1 (3) (1999) 208–219.
[4] R. Stupp, et al., Radiotherapy plus concomitant and adjuvant temozolomide for glioblastoma, N. Engl. J. Med. 352 (10) (2005) 987–996.
[5] D.R. Groothuis, The blood–brain and blood–tumor barriers: a review of strategies for increasing drug delivery, Neuro Oncol. 2 (1) (2000) 45–59.
[6] W.M. Pardridge, Blood–brain barrier drug targeting: the future of brain drug development, Mol. Interv. 3 (2) (2003) 90–105 151.
[7] R.L. Yong, et al., Human bone marrow-derived mesenchymal stem cells for intravascular delivery of oncolytic adenovirus Delta-24-RGD to human gliomas, Cancer Res. 69 (23) (2009) 8932–8940.
[8] T. Doucette, et al., Mesenchymal stem cells display tumor-specific tropism in an RCAS/Ntv-a glioma model, Neoplasia 13 (8) (2011) 716–725.
[9] T. Kosztowski, H.A. Zaidi, A. Quiñones-Hinojosa, Applications of neural and mesenchymal stem cells in the treatment of gliomas, Exp. Rev. Anticancer Ther. 9 (5) (2009) 597–612.
[10] A. Nakamizo, et al., Human bone marrow-derived mesenchymal stem cells in the treatment of gliomas, Cancer Res. 65 (8) (2005) 3307–3318.
[11] N. Shinojima, et al., TGF-β mediates homing of bone marrow-derived human mesenchymal stem cells to glioma stem cells, Cancer Res. 73 (7) (2013) 2333–2344.
[12] S.K. Singh, et al., Identification of human brain tumour initiating cells, Nature 432 (7015) (2004) 396–401.
[13] M.F. Clarke, et al., Cancer stem cells—perspectives on current status and future directions: AACR Workshop on cancer stem cells, Cancer Res. 66 (19) (2006) 9339–9344.
[14] S.K. Singh, et al., Identification of a cancer stem cell in human brain tumors, Cancer Res. 63 (18) (2003) 5821–5828.
[15] J. Lee, et al., Tumor stem cells derived from glioblastomas cultured in bFGF and EGF more closely mirror the phenotype and genotype of primary tumors than do serum-cultured cell lines, Cancer Cell 9 (5) (2006) 391–403.
[16] N. Hata, et al., Platelet-derived growth factor BB mediates the tropism of human mesenchymal stem cells for malignant gliomas, Neurosurgery 66 (1) (2010) 144–156.
[17] B.R. Son, et al., Migration of bone marrow and cord blood mesenchymal stem cells in vitro is regulated by stromal-derived factor-1-CXCR4 and hepatocyte growth factor-c-met axes and involves matrix metalloproteinases, Stem Cells 24 (5) (2006) 1254–1264.
[18] M.G. Vander Heiden, L.C. Cantley, C.B. Thompson, Understanding the Warburg effect: the metabolic requirements of cell proliferation, Science 324 (5930) (2009) 1029–1033.
[19] S.Y. Lunt, M.G. Vander Heiden, Aerobic glycolysis: meeting the metabolic requirements of cell proliferation, Annu. Rev. Cell Dev. Biol. 27 (2011) 441–464.
[20] S. Pavlides, et al., The reverse Warburg effect: aerobic glycolysis in cancer associated fibroblasts and the tumor stroma, Cell Cycle 8 (23) (2009) 3984–4001.
[21] K.M. Nieman, et al., Adipocytes promote ovarian cancer metastasis and provide energy for rapid tumor growth, Nat. Med. 17 (11) (2011) 1498–1503.
[22] W. Zhang, et al., Stromal control of cystine metabolism promotes cancer cell survival in chronic lymphocytic leukaemia, Nat. Cell Biol. 14 (3) (2012) 276–286.
[23] C.F. Lichti, et al., Integrated chromosome 19 transcriptomic and proteomic data sets derived from glioma cancer stem-cell lines, J. Proteome Res. 13 (1) (2014) 191–199.
[24] R.A. Kroes, et al., Overexpression of ST6GalNAcV, a ganglioside-specific alpha2,6-sialyltransferase, inhibits glioma growth in vivo, Proc. Natl. Acad. Sci. U. S. A. 107 (28) (2010) 12646–12651.
[25] H. He, et al., Glycomic and transcriptomic response of GSC11 glioblastoma stem cells to STAT3 phosphorylation inhibition and serum-induced differentiation, J. Proteome Res. 9 (5) (2010) 2098–2108.
[26] M. Puchades, et al., Proteomic investigation of glioblastoma cell lines treated with wild-type p53 and cytotoxic chemotherapy demonstrates an association between galectin-1 and p53 expression, J. Proteome Res. 6 (2) (2007) 869–875.
[27] S. Lal, et al., An implantable guide-screw system for brain tumor studies in small animals, J. Neurosurg. 92 (2) (2000) 326–333.
[28] A.S. Shavkunov, et al., The fibroblast growth factor 14·voltage-gated sodium channel complex is a new target of glycogen synthase kinase 3 (GSK3), J. Biol. Chem. 288 (27) (2013) 19370–19385.
[29] A.L. Oberg, O. Vitek, Statistical design of quantitative mass spectrometry-based proteomic experiments, J. Proteome Res. 8 (5) (2009) 2144–2156.
[30] C.F. Lichti, et al., Systematic identification of single amino acid variants in glioma stem-cell-derived chromosome 19 proteins, J. Proteome Res. 14 (2) (2015) 778–786.
[31] S.M. Hauck, et al., Deciphering membrane-associated molecular processes in target tissue of autoimmune uveitis by label-free quantitative mass spectrometry, Mol. Cell. Proteomics 9 (10) (2010) 2292–2305.
[32] J. Zhang, et al., PEAKS DB: de novo sequencing assisted database search for sensitive and accurate peptide identification, Mol. Cell. Proteomics 11 (4) (2012) M111.010587.
[33] X. Han, L. He, L. Xin, B. Shan, B. Ma, PeaksPTM: mass spectrometry-based identification of peptides with unspecified modifications, J. Proteome Res. 10 (7) (2011) 2930–2936.
[34] N.C. Wildburger, et al., Quantitative proteomics reveals protein–protein interactions with fibroblast growth factor12 as a component of the Nav1.2 macromolecular complex in Mammalian Brain, Mol. Cell. Proteomics (2015) .
[35] J.A. Vizcaíno, et al., The PRoteomics IDEntifications (PRIDE) database and associated tools: status in 2013, Nucleic Acids Res. 41 (2013) D1063–D1069 (Database issue).

[36] R.A. Bradshaw, A.L. Burlingame, S. Carr, R. Aebersold, Reporting protein identification data: the next generation of guidelines, Mol. Cell. Proteomics 5 (5) (2006) 787–788.
[37] K.A. Neilson, et al., Less label, more free: approaches in label-free quantitative mass spectrometry, Proteomics 11 (4) (2011) 535–553.
[38] Y. Benjamini, Y. Hochberg, Controlling the false discovery rate: a practical and powerful approach to multiple testing, J. R. Stat. Soc. B 57 (1995) 289–300.
[39] J. Cox, M. Mann, 1D and 2D annotation enrichment: a statistical method integrating quantitative proteomics with complementary high-throughput data, BMC Bioinform. 13 (Suppl. 16) (2012) S12.
[40] d.W. Huang, B.T. Sherman, R.A. Lempicki, Bioinformatics enrichment tools: paths toward the comprehensive functional analysis of large gene lists, Nucleic Acids Res. 37 (1) (2009) 1–13.
[41] D.W. Huang, B.T. Sherman, R.A. Lempicki, Systematic and integrative analysis of large gene lists using DAVID bioinformatics resources, Nat. Protoc. 4 (1) (2008) 44–57.
[42] M. Kanehisa, S. Goto, KEGG: kyoto encyclopedia of genes and genomes, Nucleic Acids Res. 28 (1) (2000) 27–30.
[43] M. Kanehisa, et al., Data, information, knowledge and principle: back to metabolism in KEGG, Nucleic Acids Res. 42 (2014) D199–D205 (Database issue).
[44] E. Mostovenko, A.M. Deelder, M. Palmblad, Protein expression dynamics during *Escherichia coli* glucose–lactose diauxie, BMC Microbiol. 11 (2011) 126.
[45] R.A. Kroes, J. Panksepp, J. Burgdorf, N.J. Otto, J.R. Moskal, Modeling depression: social dominance–submission gene expression patterns in rat neocortex, Neuroscience 137 (1) (2006) 37–49.
[46] R.A. Kroes, G. Dawson, J.R. Moskal, Focused microarray analysis of glyco-gene expression in human glioblastomas, J. Neurochem. 103 (Suppl. 1) (2007) 14–24.
[47] C.L. Nilsson, et al., Chromosome 19 annotations with disease speciation: a first report from the Global Research Consortium, J. Proteome Res. 12 (1) (2013) 135–150.
[48] G.A. Churchill, Fundamentals of experimental design for cDNA microarrays, Nat. Genet. 32 (2002) 490–495.
[49] V.G. Tusher, R. Tibshirani, G. Chu, Significance analysis of microarrays applied to the ionizing radiation response, Proc. Natl. Acad. Sci. U. S. A. 98 (9) (2001) 5116–5121.
[50] N.C. Wildburger, et al., Quantitative proteomics reveals protein–protein interactions with fibroblast growth factor 12 as a component of the voltage-gated sodium channel 1.2 (nav1.2) macromolecular complex in Mammalian brain, Mol. Cell. Proteomics 14 (5) (2015) 1288–1300.
[51] W.X. Schulze, B. Usadel, Quantitation in mass-spectrometry-based proteomics, Annu. Rev. Plant Biol. 61 (2010) 491–516.
[52] J.S. O'Brien, E.L. Sampson, Fatty acid and fatty aldehyde composition of the major brain lipids in normal human gray matter, white matter, and myelin, J. Lipid Res. 6 (4) (1965) 545–551.
[53] L. Svennerholm, Distribution and fatty acid composition of phosphoglycerides in normal human brain, J. Lipid Res. 9 (5) (1968) 570–579.
[54] S. Hong, K. Gronert, P.R. Devchand, R.L. Moussignac, C.N. Serhan, Novel docosatrienes and 17S-resolvins generated from docosahexaenoic acid in murine brain, human blood, and glial cells. Autacoids in anti-inflammation, J. Biol. Chem. 278 (17) (2003) 14677–14687.
[55] P.K. Mukherjee, V.L. Marcheselli, C.N. Serhan, N.G. Bazan, Neuroprotectin D1: a docosahexaenoic acid-derived docosatriene protects human retinal pigment epithelial cells from oxidative stress, Proc. Natl. Acad. Sci. U. S. A. 101 (22) (2004) 8491–8496.
[56] V.L. Marcheselli, et al., Novel docosanoids inhibit brain ischemia-reperfusion-mediated leukocyte infiltration and pro-inflammatory gene expression, J. Biol. Chem. 278 (44) (2003) 43807–43817.
[57] A. Ariel, C.N. Serhan, Resolvins and protectins in the termination program of acute inflammation, Trends Immunol. 28 (4) (2007) 176–183.
[58] J.M. Schwab, N. Chiang, M. Arita, C.N. Serhan, Resolvin E1 and protectin D1 activate inflammation-resolution programmes, Nature 447 (7146) (2007) 869–874.
[59] N.C. Wildburger, et al., ESI–MS/MS and MALDI-IMS localization reveal alterations in phosphatidic acid, diacylglycerol, and DHA in glioma stem cell xenografts, J. Proteome Res. 14 (June (6)) (2015) 2511–2519.
[60] O. Warburg, Uber den Stoffwechsel der Carcinomzelle, Klin. Wochenschr. 4 (1925) 534–536.
[61] O. Warburg, On the origin of cancer cells, Science 123 (3191) (1956) 309–314.
[62] R.J. DeBerardinis, et al., Beyond aerobic glycolysis: transformed cells can engage in glutamine metabolism that exceeds the requirement for protein and nucleotide synthesis, Proc. Natl. Acad. Sci. U. S. A. 104 (49) (2007) 19345–19350.
[63] J.M. Berg, J.L. Tymoczko, L. Stryer, Biochemistry, third ed., W.H. Freeman, New York, 2002.
[64] S. Langbein, et al., Expression of transketolase TKTL1 predicts colon and urothelial cancer patient survival: Warburg effect reinterpreted, Br. J. Cancer 94 (4) (2006) 578–585.
[65] R.J. Gillies, R.A. Gatenby, Adaptive landscapes and emergent phenotypes: why do cancers have high glycolysis, J. Bioenerg. Biomembr. 39 (3) (2007) 251–257.
[66] S.W. Kang, S. Lee, E.K. Lee, ROS and energy metabolism in cancer cells: alliance for fast growth, Arch. Pharm. Res. 38 (3) (2015) 338–345.
[67] K.E. Wellen, C.B. Thompson, A two-way street: reciprocal regulation of metabolism and signalling, Nat. Rev. Mol. Cell Biol. 13 (4) (2012) 270–276.
[68] S. Marshall, V. Bacote, R.R. Traxinger, Discovery of a metabolic pathway mediating glucose-induced desensitization of the glucose transport system. Role of hexosamine biosynthesis in the induction of insulin resistance, J. Biol. Chem. 266 (8) (1991) 4706–4712.
[69] M. Aebi, T. Hennet, Congenital disorders of glycosylation: genetic model systems lead the way, Trends Cell Biol. 11 (3) (2001) 136–141.
[70] J.R. Moskal, R.A. Kroes, G. Dawson, The glycobiology of brain tumors: disease relevance and therapeutic potential, Exp. Rev. Neurother. 9 (10) (2009) 1529–1545.